Ultrafast charge carrier mobility dynamics in poly(spirobifluorene-*co*-benzothiadiazole): Influence of temperature on initial transport

A. Devizis,[1] K. Meerholz,[2] D. Hertel,[2] and V. Gulbinas[1]
[1]*Center for Physical Sciences and Technology, Savanoriu 231, Vilnius, Lithuania*
[2]*Department of Chemistry, Physical Chemistry, University of Cologne, Luxemburgerstr. 116, 50939 Cologne, Germany*
(Received 27 May 2010; revised manuscript received 6 September 2010; published 15 October 2010)

In this work we examine the influence of temperature on the transport dynamics of photogenerated charge carriers in π-conjugated poly(spirobifluorene-*co*-benzothiadiazol) films. Investigations were performed by picosecond time-resolved electric field induced second-harmonic technique. The mobility is independent of temperature during the initial 100 ps. During this time, the carriers drift about 6 nm under an applied field of 1.2×10^{6} V/cm, and the mobility decreases from 3×10^{-2} cm^2/V s by one order of magnitude. We attribute this change in mobility to the intrachain charge transport during carrier relaxation down in the density of states. At a time delay of 1 ns the transport is temperature dependent with an activation energy of about 22 meV.

DOI: 10.1103/PhysRevB.82.155204 PACS number(s): 73.61.Ph, 78.47.−p, 73.50.−h

I. INTRODUCTION

The design of high-performance organic optoelectronic devices requires knowledge of technological aspects as well as fundamental phenomena. Understanding of charge transport in polymers plays a crucial role in the development of organic electronic devices. Theoretical charge transport concepts are usually verified by comparing predictions of the electric field and temperature dependence of the carrier mobility with experimental data. It is generally accepted that charge transport in amorphous organic semiconductors occurs by thermally activated carrier hopping.[1,2] The *steady-state* charge carrier mobility has been extensively investigated. Widely used mobility measurements are based on the time-of-flight (TOF) technique or current-voltage characteristics of field-effect transistors (FETs). These measurements show a decrease in carrier mobility in disordered organic semiconductors at low temperatures. The temperature dependence of the mobility varies depending on the system under investigation. Conventionally, the observed temperature dependence of the mobility follows the form of $\mu\sim\exp[-(T_0/T)^2]$, which can be rationalized within the Gaussian disorder model,[3] extensions of it,[4] or the correlated disorder model.[4] In these models the parameter T_0 is related to disorder σ, i.e., the width of the density of states (DOS). The deviation from a conventional Arrhenius activated transport is related to the temperature dependence of the equilibrium transport energy in a disordered material with a Gaussian-shaped DOS. For a detailed discussion the reader is referred to Ref. 3. Recently, it has been found that the temperature dependence of the mobility in a variety of materials is best described by an Arrhenius law $\mu\sim\exp(-\Delta/kT)$, where Δ is the activation energy.[5,6] Coropceanu *et al.*[1] claim that both relations in general fit the experimental observations within experimentally available temperature intervals.

The elucidation of the microscopic transport process is still lacking due to limited information about the dynamics of charge transport. In conventional experiments the carrier mobility is averaged in time and so the information about its dynamics is not accessible. Time-resolved investigations are necessary to obtain the details of this process. Fast time and short length scales are important because the active layers of the organic optoelectronic devices such as OLEDs or solar cells are only on the order of tens of nanometers. Consider, for example, photoexcitation of a polymer in a solar cell. The excess energy of a photon might be used to increase the mobility of carriers within tens of picoseconds after generation. On this scale dynamic effects can manifest themselves as reported in Ref. 7. Juska *et al.*[8,9] employed integral mode TOF to elucidate initial transport of photogenerated charge carriers. They obtained an initial transport distance or charge separation distance for a polythiophene derivative (RRa-PHT) and a poylfluorene derivative (PFB), which exceeded a few tens of nanometers. The initial transport on a picosecond time scale escaped determination due to limited time resolution of TOF measurements. Higher time resolution was demonstrated by Lee *et al.*,[10] who implemented photoconductivity probing with ultrashort electrical pulses by the use of the Auston strip line technique ensuring time resolution of tens of picoseconds. Their investigations revealed a fast, temperature-independent photoconductivity during the initial hundreds of picoseconds in a Poly(p-phenylene vinylene)-type polymer. This was attributed to interband charge-carrier generation.

Several attempts have been made to examine initial transport processes with better time resolution using pulse-radiolysis time-resolved microwave conductivity (TRMC)[11] or terahertz spectroscopy methods,[12] however, these techniques have serious drawbacks that limit their application. With TRMC, free carriers are probed on the molecular dimensions only, often in a liquid solution. Highly sophisticated modeling has to be used to extract information on the mobility and the obtained values are time averaged. Ultrafast terahertz spectroscopy allows time resolution of less than 1 ps,[12] but the data interpretation is not straightforward. Generally speaking, interest in the field of charge transport in organic materials remains.

Recently, we utilized the time-resolved electric field induced second-harmonic (TREFISH) generation technique for the investigation of charge transport in organic semiconductors.[13] Similarly like Stark-shift-based measurements,[14,15] the TREFISH technique enables elucida-

tion of the ultrafast electric field dynamics inside a desired material, but is more generally applicable. Manaka *et al.* also exploited electric field induced second-harmonic generation for imaging carrier drift in field-effect transistors.[16] Their technique examines carrier drift in an organic FET channel having a width of several tens of micrometers and is not applicable to time resolved investigations on the nanometer length scale. The time resolution of TREFISH, however, is only limited by the duration of the optical pulse, which allows initial charge-carrier transport to be traced by this technique. In our previous publication[13] we demonstrated the dynamic behavior of the mobility in poly(spirobifluorene-*co*-benzothiadiazole) (PSF-BT). We found the mobility decreases by five orders of magnitude following a power law $\sim t^{-\alpha}$ ($\alpha \approx 0.8$) in a time domain from picoseconds to microseconds. This fact suggests that relaxation substantially influences the mobility of photogenerated carriers. The temperature impact may be different at different stages of relaxation. Thus, clarifying this impact should help to create a more complete picture on the charge transport dynamics. In this work, we present experimental data obtained by TREFISH measurements of transient photocurrents in PSF-BT films at different temperatures.

II. METHOD AND EXPERIMENT

A. Experiment

PSF-BT was obtained from Merck KGaA. A polymer film of 100 nm thickness was spin coated from 10 g/l solution in toluene on indium tin oxide (ITO) covered glass. The ITO was cleaned using standard procedures. A 100-nm-thick aluminum electrode was thermally evaporated on the polymer film at a pressure of 10^{-6} mbar. The measured capacitance of the device was 1.5 nF, which is in good agreement with the estimation from the sample area and thickness. The optical density of the film was approximately 0.2 at the excitation wavelength of 500 nm, which is the red edge of the PSF-BT absorption band. Therefore, excitation can be assumed to be homogenous within the film thickness. The neutral polymer does not absorb at the probe wavelength of 810 nm.

All pump-probe measurements were done using a femtosecond spectrometer based on the amplified Ti-Sapphire laser Quantronics "*Integra C*" (130 fs pulse width, 810 nm wavelength, 1 kHz repetition rate) and equipped with the parametric generator "*TOPAS C.*" The experimental scheme is depicted in Fig. 2. The fundamental beam (810 nm) passed through the delay stage and the sample, and was reflected from the aluminum electrode. Second harmonic intensity (405 nm) was detected with a photomultiplying tube using a bandpass filter. A mechanical chopper was used for modulation of the pump beam and the signal was detected in differential mode retrieving the ratio of second-harmonic intensities with and without excitation, respectively. The external voltage was applied using a square wave pulse generator synchronized to the laser pulses. In order to minimize carrier injection from electrodes, a positive bias was applied to the aluminum electrode. The pulses were set to a duration of tens of microseconds and 12 V amplitude, which corresponds to

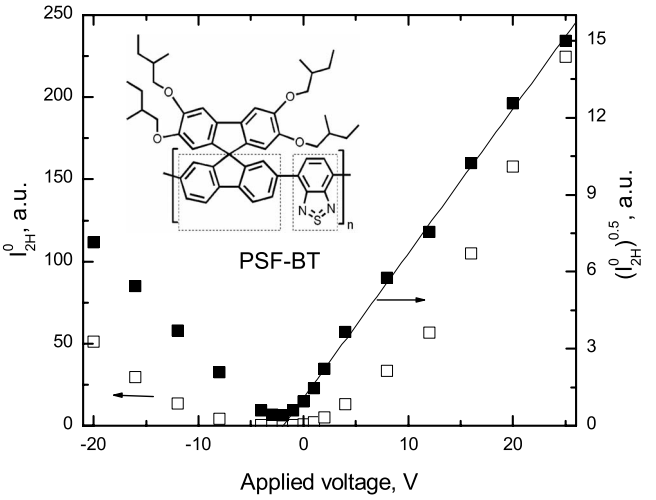

FIG. 1. The voltage dependence of the second-harmonic (405 nm) intensity I^0_{2H} (□) and $\sqrt{I^0_{2H}}$ (■) of PSF-BT. The straight line is a fit according to Eq. (1). The inset shows the backbone structure of the PSF-BT.

an electric field of 1.2×10^6 V/cm in the polymer film. The photocurrent was measured with an oscilloscope using an external electrical circuit. The large capacitance of the sample prevented current-mode measurement. Only the time-integrated value of the photocurrent $\Delta q(t > \tau_{extr})_{cc}$ was obtained. Temperature control was performed by a liquid-helium closed cycle cryostat "Janis CCS-100/204."

B. Investigation method

Briefly, the concept of TREFISH is as follows. In a sandwich-type organic electronic devices the material fills the space between electrodes forming a plate capacitor-like device. If this capacitor is charged and exposed to light pulses, the drifting photogenerated charge carriers subsequently discharge the capacitor and the electric field in the material declines. One can observe the voltage kinetics by electrical measurements. However, time resolution of electrical measurements is limited to subnanoseconds in the best case. The investigated material itself can be used as a probe to measure the electric field strength optically if some of its optical properties depend on electric field.

The TREFISH method enables measurement of the electric field strength inside the investigated materials by means of optical second-harmonic generation (SHG). It is based on

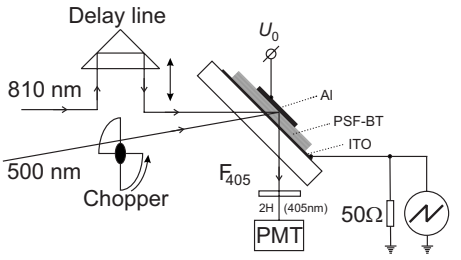

FIG. 2. The experimental setup used to measure TREFISH and time-integrated photocurrent (probe: 810 nm, pump: 500 nm).

a well-known EFISH generation phenomenon, which is commonly used for the determination of the molecular hyperpolarizability.[17,18] This phenomenon was also used for the investigation of the electric field dynamics on surfaces and interfaces of inorganic semiconductors.[19–21] An applied electric field breaks the centrosymmetry of an amorphous polymer and SHG is obtained from the polymer film. The SHG efficiency is proportional to the hyperpolarizability of the molecules[17,18] and to the second power of the applied field. Thus, the electric field E inside the investigated material can be monitored by measuring the second-harmonic intensity (I_{2H}^0),

$$E \sim \sqrt{I_{2H}^0}. \tag{1}$$

Figure 1 shows experimental evidence for the validity of Eq. (1) for PSF-BT. For the results in Fig. 1 810 nm light pulses (150 fs) have been used as probe, thus I_{2H}^0 is light generated at 405 nm. The square root of the second-harmonic intensity obeys a linear dependence on the external voltage applied to the device. The minimum intensity is shifted to negative voltage due to the built-in electric field, arising from the difference of work functions of the aluminum and ITO electrodes. The capacitor-like device, charged in advance by an external electric supply, is discharged by the photocurrent. Thus, the photocurrent reduces the initial electric field $E_0 = U_0/d$, here U_0 and d are the external voltage and polymer layer thickness, respectively. The measurement is carried out in a pump-probe scheme (Fig. 2). The pump pulse (500 nm) creates charge carriers and the subsequent probe pulse (810 nm) senses the electric field strength in the polymer film. The electric field dynamics $\Delta E(t)$ may be obtained by changing time delay t between pump and probe pulses. In the case of relatively small field variations compared with E_0, the time-dependent $I_{2H}(t)$ relates to $\Delta E(t)$ as

$$\Delta E(t) \approx \{[I_{2H}(t)/I_{2H}^0]^{1/2} - 1\}E_0, \tag{2}$$

where I_{2H}^0 is the second-harmonic intensity without a pump pulse. The time resolution of the measurement is limited only by the duration of the optical pulses applied for excitation and probing. Drift of photogenerated charge carriers creates the photocurrent and the field-induced polarization of photogenerated neutral excitons creates the displacement current. Therefore, the change in the electric field can be expressed as the sum of the exciton $\Delta E(t)_{exc}$ and charge-carrier $\Delta E(t)_{cc}$ contributions,

$$\Delta E(t) = \Delta E(t)_{exc} + \Delta E(t)_{cc}. \tag{3}$$

If the field change is small in comparison with the applied field the exciton contribution may be approximately expressed as

$$\Delta E_{exc}(t) \approx -n(t)_{exc}(\Delta\alpha)E_0/2\varepsilon\varepsilon_0, \tag{4}$$

where $n(t)_{exc}$ is the exciton density, $\Delta\alpha$ is the change in the polarizability of the excited chain or chain segment with respect to the ground state, ε is the dielectric constant of the material, and ε_0 is the permittivity of free space. Due to their large polarizability, excitons cause a rapid decrease in the field and, thus, reduce the second-harmonic intensity during the excitation pulse action; the field recovers when the excitons decay (for example, see Fig. 3, data obtained at 2 V). Their time-integrated contribution to the transported charge is zero. The exciton contribution dominates the $\Delta E(t)$ kinetics at low applied voltages when the charge carrier generation yield is low.[13] Since $\Delta E(t)_{exc}$ is proportional to the exciton density, its kinetics may be obtained from time-resolved fluorescence or transient absorption measurements. Proportionality of $\Delta E(t)_{exc}$ to the applied electric field helps to determine its absolute value by measuring the electric field kinetics at different applied voltages, which was demonstrated in Ref. 22.

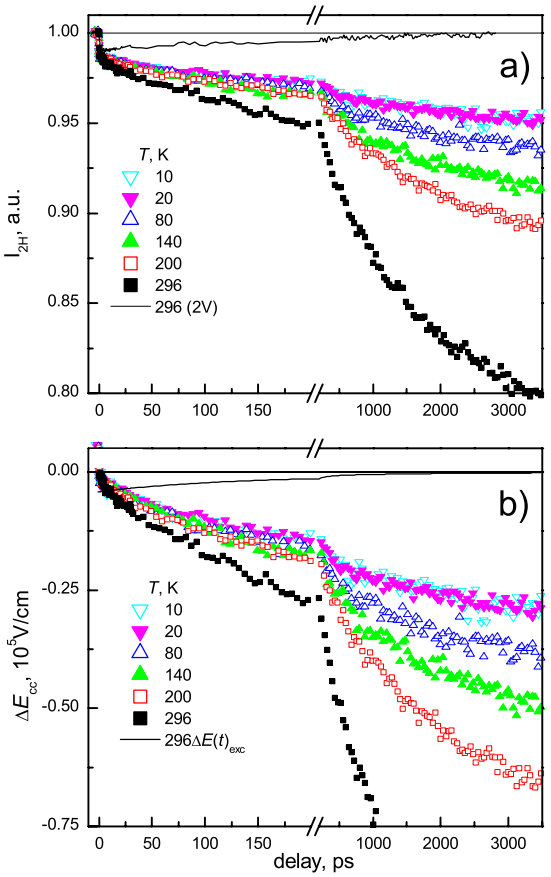

FIG. 3. (Color online) (a) The dependence of the second-harmonic intensity I_{2H} on the probe pulse delay with respect to the pump pulse (500 nm) at different temperatures and 12 V (see legend). The line is the result at 2 V. The second-harmonic intensity I_{2H} is normalized to the second-harmonic intensity without excitation I_{2H}^0. (b) Field drop $\Delta E(t)_{cc}$ related to the charge-carrier drift at different temperatures (symbols) and the exciton contribution (displacement) $\Delta E(t)_{exc}$ at room temperature (solid line).

The charge-carrier contribution may be expressed as

$$\Delta E(t)_{cc} = \Delta q(t)_{cc}/Cd = \frac{1}{Cd}\int_0^t j(t')dt', \tag{5}$$

where $\Delta q(t)_{cc}$ is the amount of the transported charge, C is the sample capacitance, and $j(t)$ is the time-dependent photocurrent. We can express $\Delta E(t)_{cc}$ by the average drift dis-

tance $\langle l(t)\rangle$ and the density $n(t)_{cc}$ of photogenerated charge carriers,

$$\Delta E(t)_{cc} = n(t)_{cc} e \langle l(t)\rangle / \varepsilon\varepsilon_0, \tag{6}$$

where e is the elementary charge. Carriers are extracted from the sample at long time τ_{extr}. If carriers are generated homogeneously within the sample, the electrically measured (external) field drops at $t > \tau_{extr}$, which can be measured electrically,

$$\Delta E(t > \tau_{extr})_{cc} = n^0_{cc} e d / 2\varepsilon\varepsilon_0, \tag{7}$$

where n^0_{cc} is the final concentration of the carriers at the end of generation process. With the knowledge of n^0_{cc} we can determine the time dependence of the average drift distance as

$$\langle l(t)\rangle = \frac{n^0_{cc}}{n(t)_{cc}} \frac{\Delta E(t)_{cc}}{\Delta E(t > \tau_{extr})_{cc}} \frac{d}{2}. \tag{8}$$

It should be noted that the average drift distance determined in this way is averaged over all electrons and holes. If carriers of one sign move much faster, the initial field kinetics is determined by faster moving carriers, while slower carriers determine the field kinetics at long times. The photocurrent depends on the concentration of generated carriers and on their mobility. The average carrier mobility may be found relying on the photocurrent and carrier density data as

$$\mu(t) = \frac{j(t)}{A E_0 n(t)_{cc} e}, \tag{9}$$

where A is the sample area. Photocurrent is obtained by differentiating the experimentally measured $\Delta E(t)_{cc}$, as follows from Eq. (5). Subsequently by using Eq. (9) and expressing the constants via Eq. (7), we obtain the carrier mobility,

$$\mu(t) = \frac{n^0_{cc}}{n(t)_{cc}} \frac{D}{2E_0 \Delta E(t > \tau_{extr})_{cc}} \frac{d\Delta E(t)_{cc}}{dt}. \tag{10}$$

The latter equation does not account for carrier extraction from the sample and, thus, loses accuracy as $\langle l(t)\rangle$ approaches $d/2$. At shorter times, $n_{cc}(t)$ varies due to carrier generation, which may be obtained from time-resolved electric field induced fluorescence quenching[23] or electric field modulated transient absorption investigations.[14]

III. RESULTS

TREFISH measurements give $I_{2H}(t)$ as a function of delay time between excitation and probe pulses. Raw experimental data, parametric in temperature, is presented in Fig. 3(a). The signal is normalized to I^0_{2H} without excitation pulse, thus the ratio is unity at negative delays, when the probe pulse arrives prior to the excitation pulse. There is a step-like drop of the $I_{2H}(t)$ at zero delay time. Later, the $I_{2H}(t)$ signal gradually continues to decay. The $I_{2H}(t)$ decays more rapidly at higher temperatures, which becomes more pronounced at longer delay times. The temperature effect becomes negligible at low temperatures; there is no difference between curves obtained at 10 and 20 K. This data was used to calculate the electric field kinetics by using Eq. (2). Figure 3(b) shows the electric field kinetics separated into the charge-carrier and exciton contributions. The exciton contribution was estimated and subtracted from the electric field kinetics on the basis of the fluorescence decay kinetics by the same procedure used in Ref. 13. Briefly, $I_{2H}(t)$ were measured at low applied voltages [2 V, Fig. 3(a)] where the carrier generation is negligible (see discussion below). The shape of the corresponding electric field kinetics is very similar to the fluorescence kinetics, confirming the dominance of the exciton contribution for the field kinetics. The exciton contribution at higher fields was obtained by multiplying the field kinetics obtained at low field (2×10^5 V/cm, Fig. 3) by the actual applied field according to Eq. (4). The exciton decay kinetics only weakly depend on temperature.[24] Therefore, we used the same exciton contribution at all temperatures.

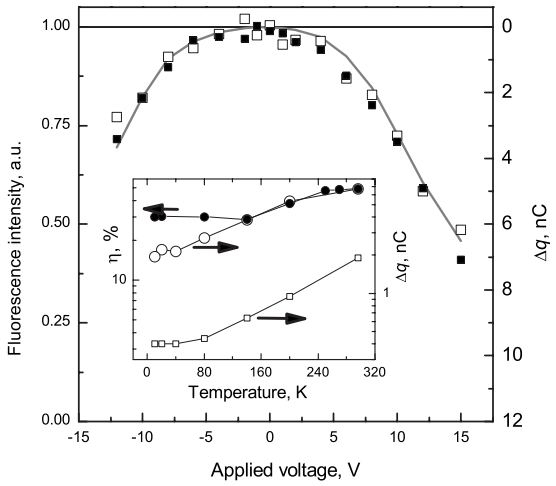

FIG. 4. Fluorescence quenching by an external voltage at two different excitation wavelengths (■—360 nm, □—500 nm). The integrated photocurrent is represented by the gray line. The inset shows the fluorescence quenching efficiency η (●) (Ref. 25), the amount of the collected charge $\Delta q(t > \tau_{extr})$ (○) versus temperature, and the empty squares (□) represent values of Δq(3.5 ns) obtained by TREFISH at 3.5 ns.

It is crucial to know the final density of photogenerated charge carriers n^0_{cc} in order to calculate the average drift distance and the average mobility. n^0_{cc} was obtained from a combination of electrical measurements corresponding to photogenerated and extracted charge and electric field assisted fluorescence quenching data. Figure 4 compares the voltage dependence of the total extracted charge and fluorescence quenching at room temperature, which are identical within experimental accuracy. This finding indicates that (i) all quenched excitons produced charge carriers and (ii) all photogenerated carriers were extracted from the sample. Thus, the extracted charge is a valid measure of the photogenerated charge density at room temperature. The density at lower temperatures was obtained from the carrier generation investigation.[25]

The situation slightly changes at low temperatures, where both, the fluorescence quenching and the extracted charge density decrease (see inset in Fig. 4). Both values decrease proportionally down to about 140 K. However, at lower tem-

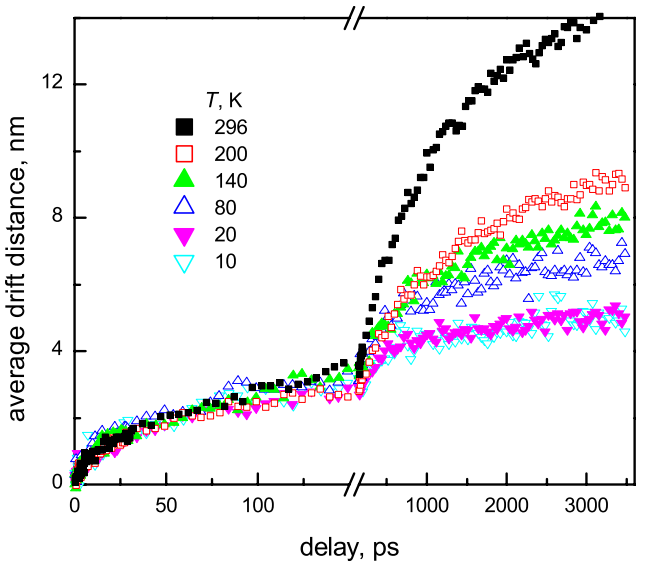

FIG. 5. (Color online) Average charge carrier drift distance versus time delay after photoexcitation at different temperatures.

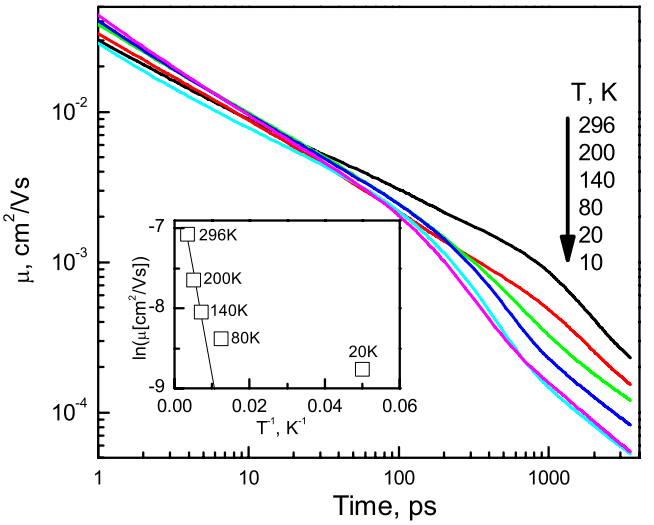

FIG. 6. (Color online) Carrier mobility at different temperatures obtained by calculating the temporal derivative of the carrier contribution to the electric field dynamics. The inset shows the Arrhenius plot of the carrier mobility at 1 ns. The line at higher temperatures is a fit to the Arrhenius law, which gives an activation energy of 22 meV.

peratures, the amount of extracted charge continues to decrease while fluorescence quenching is constant. Evidently, not all charge carriers are extracted at low temperatures. Comparison of the temperature dependence of the extracted charge and fluorescence quenching suggests that about 50% of carriers remain trapped at 40 K and below. Thus, the electrically measured extracted charge becomes an inadequate measure of the amount of the photogenerated charge at low temperatures. Therefore, we assumed that the amount of photogenerated charge follows the same temperature dependence as the fluorescence quenching. Calculation of the average drift distance and carrier mobility described below supports this assumption. If we assume that the generated charge at all temperatures equals the electrically measured charge, we would obtain an increase in the drift distance and carrier mobility at very low temperatures, which is completely irrational. The inset in Fig. 4 shows the amount of drifted charge at 3.5 ns measured by the TREFISH method. This amount is about five to seven times smaller than the electrically measured charge at long time τ_{extr} and room temperature.

The calculated average drift distances are shown in Fig. 5. We calculated the average drift distance by Eq. (8). The time-dependent carrier density, needed for mobility calculations (see below), was estimated from carrier generation data presented in Ref. 25. There we concluded the majority of charge is already generated during the first picosecond after excitation. The time scale of carrier drift starts at 1 ps (Fig. 5) and the drift distance starts at zero. Thus, the initial charge carrier separation on a subpicosecond time scale here is not accounted for. Several important features of the charge drift are apparent in Fig. 5. First of all, it is evident that the carrier motion is independent of temperature during the first 100 ps. Later on, the transport is temperature activated. At room temperature, charge carriers move rapidly and are one third (33 nm) the way toward the electrode after 3.5 ns. The motion slows down at lower temperatures. A decrease in temperature from 296 to 80 K causes a gradual reduction of the drift distance. At 10 and 20 K the curves are identical within the entire time interval under investigation, implying that temperature activation does not govern charge transport at low temperatures. We note that the drift distance during the first 100 ps or so is approximately 3 nm, which is almost as much over the next 3 ns at 10 and 20 K.

Figure 6 shows the carrier mobility dynamics calculated using Eq. (10). In order to avoid large errors generated by data differentiation, the electric field kinetics were approximated by multiexponential functions and differentiated afterward. The carrier mobility drops by one order of magnitude during the initial 100 ps; however, the mobility values and decay rate were independent of temperature. A clear temperature dependence appears on a subnanosecond time scale. A more rapid decrease in mobility at nanosecond times is observed at lower temperatures.

IV. DISCUSSION

A typical transport analysis in amorphous molecular systems is based on the disorder model.[2,3] This model describes the material being composed of randomly distributed molecular sites with different energies. Sites can be subunits of the polymer and/or functional parts of molecules. The energy difference arises from varying conjugation length and polarization effects of the surrounding due to random fluctuations of the van der Waals interactions. If we apply the disorder model to rationalize charge transport in PSF-BT, the charge carrier hops from site to site are determined by the energy difference and coupling between sites. It is reasonable to assume that carriers gradually occupy lower and lower energy sites during their drift and diffusional motion. Therefore, carrier hops on a subnanosecond time scale are likely to take place between the high-energy states and the thermal

equilibrium states in the DOS and thus transport weakly depends on temperature. Temperature independent relaxation within DOS at the initial stage of carrier diffusion has been demonstrated by means of Monte Carlo modeling.[26] The strong temperature dependence of the carrier mobility appears on a nanosecond time scale, when carriers reach low-energy sites and charge transport takes place in equilibrium. Temperature activation starts to play an integral role since carriers have to be activated to the transport energy (close to the center of the DOS) to be transported. Temperature-dependent mobility values are depicted in an Arrhenius plot (Fig. 6). From the slope of the high-temperature asymptote an activation energy of 22 meV can be calculated. The activation energy is much smaller than a typical value of the width of the DOS in polymers [100 meV (Ref. 2)], implying the site from which transport proceeds lies within the DOS. This relatively low activation energy indicates that the carriers at about 1 ns delay time are still not localized into the tail of the DOS (equilibrium energy) or deep traps and the steady state drift regime is not established. Deviation from standard Arrhenius behavior (Fig. 6) took place at low temperatures, likely due to turnover from temperature activated to tunneling transfer.

Although the disorder model gives a qualitative explanation of the temperature-independent initial charge transport, conjugated polymers have a more complex microscopic structure, which evidently plays a significant role in the charge transport at short distances. Conjugated polymers chains are composed of conjugated segments with a length of about 5–10 nm. These conjugated segments are separated by structural defects creating barriers for carrier motion. Carrier transport along the polymer chain (*intrachain*) and between chains (*interchain*) is expected to be rather different because of different electron wave function overlap between conjugated segments and polymer chains. For intrachain motion, we have to distinguish between two transport mechanisms. (i) Along a conjugated segment, the transport is expected to be coherent and very fast. This is based on calculations of the effective carrier mass in conjugated polymers.[4] A value of $0.1m_e$ has been found, in accordance with electroabsorption measurements in polydiacetylene,[27] translating to a potential mobility as high as 1000 $cm^2/V\,s$. The astonishingly high mobility of 600 $cm^2/V\,s$ in ladder-type poly(phenylene) (Ref. 28) might correspond to transport along a conjugated segment of about 5 nm length. In PSF-BT the mobility at room temperature is on the order of $(10^{-1}-10^{-2})cm^2/V\,s$ even on a time scale of several picoseconds.[13] Thus (ii) incoherent carrier transport between conjugated segments of PSF-BT is more plausible.

Commonly, incoherent charge transport consists of two contributions: temperature-activated hopping and tunneling transfer. Tunneling transport, which is weakly temperature dependent, usually dominates at lower temperatures. We suggest that structural defects in the polymer chains forming positional traps create barriers for the carrier motion. The electron wave functions of neighboring conjugated segments of the same polymer chain evidently still overlap strongly enough that carrier hops occur by tunneling and need no thermal assistance.[1] Additional support for incoherent initial transport comes from electrochemical and quantum chemical investigations of PSF-BT.[25] Right after photogeneration, holes in PSF-BT polymer are localized (trapped) on a single spiroconjugated fluorene side group and the electron wave function is delocalized on the backbone, mainly on BT groups.[25] Although delocalization of the electron wave function is relatively weak because of disordered polymer chain structure,[29] the electron mobility in PSF-BT is much higher than mobility of holes. Time-of-flight measurements on 3.6-μm-thick PSF-BT films show that the steady-state electron mobility is $6\times10^{-4}-3\times10^{-3}$ $cm^2/V\,s$ at an electric field of 10^5-10^6 V/cm, and the hole mobility is two orders of magnitude lower, ranging from 3×10^{-6} to 5×10^{-5} $cm^2/V\,s$.[30] Thus, the fast initial charge drift evidently corresponds only to the electron motion. The temperature independent drift distance of about 3 nm (Fig. 5) obtained from TREFISH measurements is averaged over both electrons and holes. Since holes are immobile on the ultrafast time scale, from the 3 nm drift distance a temperature independent electron drift distance of about 6 nm follows. The average charge drift of only about 6 nm during this transport phase seems to be relatively short considering the length of a polymer chain of tens of nanometers. However, one has to keep in mind this drift distance is a projection of the total drift distance to the electric field direction. Assuming a random polymer chain orientation the total intrachain carrier drift should be at least two times larger. This distance may be even larger if the polymer chains are dominantly oriented along the film plane, as one may expect a the spin-cast film. Thus, the total drift distance may be on the order of 12 nm or larger, which is a reasonable value for intrachain motion between conjugated segments.

Carrier hops between different chains, i.e., interchain motion, are considered as hops through/over barriers, which are probably higher than the intrachain barriers. The interchain carrier hops are much slower and need temperature assistance.[2,3] The interchain motion is governed by the energetic and positional polymer disorder, which determines the macroscopic carrier mobility. Identical carrier motion dynamics at 10 and 20 K suggest carrier tunneling is responsible for the transport at very low temperatures as well. This is consistent with the observations of the temperature-independent macroscopic transport at low temperatures.[31]

So far it is difficult to unambiguously determine which factor plays a dominant role in the temperature-independent initial transport. According to calculations presented in Ref. 32, triplet exciton diffusivity kinetics at different temperatures start to deviate only when approaching equilibrium. We expect the same for charge carriers since both triplet excitons and charges hop by electron exchange as opposed, for instance, to singlet excitons. Mobility dynamics (Fig. 6), however, gain temperature dependence much faster than equilibrium is reached; we do not see the system reach equilibrium in the investigated time interval; the mobility constantly decreases. Therefore, the relaxation within the DOS in the conventional model[2,3] can hardly explain the observed temperature dependence of the charge mobility dynamics. The hierarchical structure of conjugated polymers evidently is also important. This hierarchical carrier motion—inside well-ordered polymer segments, between these segments and between polymer chains—causes a rapid mobility decay,

where the temperature-independent phase indicates that lower barriers at least are overcome by carrier tunneling rather than by thermal activation.

It is instructive to compare our results with transient photocurrent measurements[7,10,33–35] where a temperature-independent photocurrent was obtained by conductivity probing with short electrical pulses generated by the Auston switch technique. These results are confirmed by our data. However, one has to keep in mind that the time resolution of our experiments is by two orders of magnitude higher, giving the possibility to resolve the ultrafast photocurrent dynamics. We were able to obtain more details of the carrier drift kinetics. First of all, our experiments revealed that the carrier mobility changes by about two orders of magnitude during the temperature-independent transport phase. This fact requires a slightly different interpretation of our results based on the hierarchical carrier motion. Carrier trapping as suggested by Heegers group cannot fully explain this transport behavior. Trapping in a conventional sense requires establishment of thermal equilibrium and the existence of traps that are deep compared with the width of the DOS. We do not observe this kind of trapping. If trapping is identified with polaron relaxation as it is discussed in Ref. 35, the temperature dependence at nanosecond times may be considered trapping. This however, requires direct free-carrier generation. Currently we have not sufficient evidence for free-carrier generation in our materials.

V. SUMMARY AND CONCLUSIONS

The time-resolved electric field induced second-harmonic method was used to investigate the influence of temperature on photogenerated charge carrier transport in PSF-BT. We demonstrated the temperature-independent initial drift of photogenerated charge carriers. Turnover from temperature-independent to activated carrier drift takes place on the time scale of about 100 ps and an average drift distance of about 6 nm. We relate the temperature-independent transport to tunneling through energy barriers, resembling relaxation of carriers within the DOS. At longer times, temperature assists charge transport and our results are consistent with thermally activated hopping. At low temperatures (10 and 20 K) charge movement at a nanosecond time scale is negligible, most probably due to the trapping at the bottom of DOS.

ACKNOWLEDGMENTS

We would like to acknowledge C. R. Shallcross for helpful suggestions concerning the manuscript. The work was supported by the Research Council of Lithuania and the German Science Foundation (DFG) (Grant No. HE 5577/1).

[1] V. Coropceanu, J. Cornil, D. A. da Silva Filho, Y. Olivier, R. Silbey, and J. L. Bredas, Chem. Rev. **107**, 926 (2007).
[2] D. Hertel and H. Bässler, ChemPhysChem **9**, 666 (2008).
[3] H. Bässler, Phys. Status Solidi B **175**, 15 (1993).
[4] J. W. van der Horst, P. A. Bobbert, M. A. J. Michels, and H. Bässler, J. Chem. Phys. **114**, 6950 (2001).
[5] P. W. M. Blom, M. J. M. de Jong, and M. G. van Munster, Phys. Rev. B **55**, R656 (1997).
[6] N. I. Craciun, J. Wildeman, and P. W. M. Blom, Phys. Rev. Lett. **100**, 056601 (2008).
[7] D. Moses, J. Wang, G. Yu, and A. J. Heeger, Phys. Rev. Lett. **80**, 2685 (1998).
[8] G. Juška, K. Genevičius, R. Österbacka, K. Arlauskas, T. Kreouzis, D. D. C. Bradley, and H. Stubb, Phys. Rev. B **67**, 081201(R) (2003).
[9] R. Österbacka, K. Genevičius, A. Pivrikas, G. Juška, K. Arlauskas, T. Kreouzis, D. D. C. Bradley, and H. Stubb, Synth. Met. **139**, 811 (2003).
[10] C. H. Lee, G. Yu, D. Moses, and A. J. Heeger, Phys. Rev. B **49**, 2396 (1994).
[11] R. J. O. M. Hoofman, M. P. de Haas, L. D. A. Siebbeles, and J. M. Warman, Nature (London) **392**, 54 (1998).
[12] E. Hendry, M. Koeberg, J. M. Schins, H. K. Nienhuys, V. Sunstrom, L. D. A. Siebbeles, and M. Bonn, Phys. Rev. B **71**, 125201 (2005).
[13] A. Devižis, A. Serbenta, K. Meerholz, D. Hertel, and V. Gulbinas, Phys. Rev. Lett. **103**, 027404 (2009).
[14] V. Gulbinas, Y. Zaushitsyn, V. Sundström, D. Hertel, H. Bässler, and A. Yartsev, Phys. Rev. Lett. **89**, 107401 (2002).
[15] J. Cabanillas-Gonzalez, T. Virgili, A. Gambetta, G. Lanzani, T. D. Anthopoulos, and D. M. de Leeuw, Phys. Rev. Lett. **96**, 106601 (2006).
[16] T. Manaka, E. Lim, R. Tamura, and M. Iwamoto, Nat. Photonics **1**, 581 (2007).
[17] C. Bosshard, G. Knöpfle, P. Pretre, and P. Günter, J. Appl. Phys. **71**, 1594 (1992).
[18] J. W. Perry, in *Materials for Nonlinear Optics*, edited by S. R. Marder, E. J. Sohn, and G. D. Stucky (American Chemical Society, Washington, 1991).
[19] R. M. Corn and D. A. Higgins, Chem. Rev. **94**, 107 (1994).
[20] Yu. D. Glinka, T. V. Shahbazyan, I. E. Perakis, N. H. Tolk, X. Liu, Y. Sasaki, and J. K. Furdyna, Appl. Phys. Lett. **81**, 3717 (2002).
[21] Y. D. Glinka, W. Wang, S. K. Singh, Z. Marka, S. N. Rashkeev, Y. Shirokaya, R. Albridge, S. T. Pantelides, N. H. Tolk, and G. Lucovsky, Phys. Rev. B **65**, 193103 (2002).
[22] A. Devižis, A. Serbenta, D. Hertel, and V. Gulbinas, Mol. Cryst. Liq. Cryst. **496**, 16 (2008).
[23] D. Hertel, E. V. Soh, H. Bässler, and L. J. Rothberg, Chem. Phys. Lett. **361**, 99 (2002).
[24] A. Devižis, A. Serbenta, K. Meerholz, D. Hertel, and V. Gulbinas, J. Chem. Phys. **131**, 104902 (2009).
[25] A. Devizis, A. Serbenta, D. Peckus, A. Thiessen, R. Alle, K. Meerholz, D. Hertel, and V. Gulbinas, J. Chem. Phys. (to be published).
[26] B. Movaghar, M. Grünewald, B. Ries, H. Bässler, and D. Würtz, Phys. Rev. B **33**, 5545 (1986).
[27] G. Weiser and S. Möller, Phys. Rev. B **65**, 045203 (2002).

[28] P. Prins, F. C. Grozema, J. M. Schins, T. J. Savenije, S. Patil, U. Scherf, and L. D. A. Siebbeles, Phys. Rev. Lett. **96**, 146601 (2006).
[29] M. Wohlgenannt, X. M. Jiang, and Z. V. Vardeny, Phys. Rev. B **69**, 241204(R) (2004).
[30] See supplementary material at http://link.aps.org/supplemental/10.1103/PhysRevLett.103.027404 for supporting information.
[31] G. Horowitz, M. E. Hajlaoui, and R. Hajlaoui, J. Appl. Phys. **87**, 4456 (2000).
[32] R. Richert and H. Bässler, Chem. Phys. Lett. **118**, 235 (1985).
[33] D. Moses, H. Okumoto, C. H. Lee, A. J. Heeger, T. Ohnishi, and T. Noguchi, Phys. Rev. B **54**, 4748 (1996).
[34] C. H. Lee, J. Y. Park, Y. W. Park, D. Moses, A. J. Heeger, T. Noguchid, and T. Ohnishid, Synth. Met. **101**, 444 (1999).
[35] M. Tong, N. E. Coates, D. Moses, A. J. Heeger, S. Beaupre, and M. Leclerc, Phys. Rev. B **81**, 125210 (2010).